

# *Wolbachia* Modulates Lipid Metabolism in *Aedes albopictus* Mosquito Cells

Jennifer C. Molloy,<sup>a</sup> Ulf Sommer,<sup>b</sup> Mark R. Viant,<sup>b</sup> Steven P. Sinkins<sup>a,c</sup>

Nuffield Department of Medicine and Department of Zoology, University of Oxford, Oxford, United Kingdom<sup>a</sup>; NERC Biomolecular Analysis Facility—Metabolomics Node, School of Biosciences, University of Birmingham, Birmingham, United Kingdom<sup>b</sup>; Biomedical and Life Sciences, Lancaster University, Lancaster, United Kingdom<sup>c</sup>

## ABSTRACT

Certain strains of the intracellular endosymbiont *Wolbachia* can strongly inhibit or block the transmission of viruses such as dengue virus (DENV) by *Aedes* mosquitoes, and the mechanisms responsible are still not well understood. Direct infusion and liquid chromatography-Fourier transform ion cyclotron resonance (FT-ICR) mass spectrometry-based lipidomics analyses were conducted using *Aedes albopictus* Aa23 cells that were infected with the *wMel* and *wMelPop* strains of *Wolbachia* in comparison to uninfected Aa23-T cells. Substantial shifts in the cellular lipid profile were apparent in the presence of *Wolbachia*. Most significantly, almost all sphingolipid classes were depleted, and some reductions in diacylglycerols and phosphatidylcholines were also observed. These lipid classes have previously been shown to be selectively enriched in DENV-infected mosquito cells, suggesting that *Wolbachia* may produce a cellular lipid environment that is antagonistic to viral replication. The data improve our understanding of the intracellular interactions between *Wolbachia* and mosquitoes.

## IMPORTANCE

Mosquitoes transmit a variety of important viruses to humans, such as dengue virus and Zika virus. Certain strains of the intracellular bacterial genus called *Wolbachia* found in or introduced into mosquitoes can block the transmission of viruses, including dengue virus, but the mechanisms responsible are not well understood. We found substantial shifts in the cellular lipid profiles in the presence of these bacteria. Some lipid classes previously shown to be enriched in dengue virus-infected mosquito cells were depleted in the presence of *Wolbachia*, suggesting that *Wolbachia* may produce a cellular lipid environment that inhibits mosquito-borne viruses.

*Wolbachia* endosymbionts are common intracellular, maternally inherited bacteria that manipulate host reproduction. The most common form of manipulation is cytoplasmic incompatibility (CI), patterns of crossing sterile individuals that can provide a reproductive advantage to females carrying the bacteria, allowing rapid population spread and maintenance at high frequency (1). In certain host-strain combinations, in particular where high bacterial densities are reached, *Wolbachia* can significantly reduce the transmission of some of the most important mosquito-borne pathogens of humans, including dengue (DENV) and Chikungunya viruses and malaria and filarial nematode parasites (2–10). The *wMel* strain of *Wolbachia pipiensis* has been used for field trials in *Aedes aegypti* mosquitoes, having reached and remained at a very high population frequency (11, 12), and wild carriers still show greatly reduced DENV susceptibility several years later (13). The mechanisms behind the pathogen inhibition phenotype remain uncertain; upregulation of innate immune genes has been observed and can contribute to the phenotype (2–5, 9, 14) but is apparently not required for efficient viral transmission blocking (7, 8, 15).

The cellular lipidome often undergoes major changes in the presence of pathogens, as seen for mosquito cells infected with DENV; inhibition of fatty acid synthase at 4 to 12 h after DENV infection results in greatly reduced viral titers (16). In mammalian cells, autophagy-mediated release of triglyceride fatty acids from lipid droplets is required for DENV replication (17–21). Cholesterol can also play an important role in arbovirus entry to mammalian cells (22–25), viral envelope formation (17), and exit from the cell (26). Lipid metabolism and autophagy are not only impli-

cated in pathogen-mosquito interactions but are likely to be critical to the *Wolbachia*-host relationship. The streamlined genome of *Wolbachia* lacks synthesis pathways for fatty acids and cholesterol (27), so *Wolbachia*-host symbioses provide a likely arena for resource competition that could in turn impact viral refractoriness. Insects can synthesize fatty acids and other lipid classes but are also sterol auxotrophs (28), increasing the potential for competition over dietary cholesterol. Cholesterol modulation by *Wolbachia* has already been suggested to play a functional role in DENV infection in *wMel*-infected *Drosophila melanogaster* flies, where increased dietary cholesterol reduced viral refractoriness (29), but any role in mosquitoes remains an open question.

The influence of *Wolbachia* on broader host lipid metabolism remains unknown, as few data have been published, but there are potential mechanistic links. Autophagy is known to alter lipid

Received 27 January 2016 Accepted 10 March 2016

Accepted manuscript posted online 18 March 2016

Citation Molloy JC, Sommer U, Viant MR, Sinkins SP. 2016. *Wolbachia* modulates lipid metabolism in *Aedes albopictus* mosquito cells. *Appl Environ Microbiol* 82:3109–3120. doi:10.1128/AEM.00275-16.

Editor: P. D. Schloss, University of Michigan

Address correspondence to Steven P. Sinkins, s.sinkins@lancaster.ac.uk.

J.C.M. and U.S. contributed equally to this article.

Supplemental material for this article may be found at <http://dx.doi.org/10.1128/AEM.00275-16>.

Copyright © 2016 Molloy et al. This is an open-access article distributed under the terms of the [Creative Commons Attribution 4.0 International license](https://creativecommons.org/licenses/by/4.0/).

profiles and has been shown to reduce *Wolbachia* density if up-regulated, leading to the suggestion that *Wolbachia* might modulate the process in hosts (30). As DENV requires autophagy for replication, this is interesting in the context of *wMel*-infected *D. melanogaster* flies, which are protected against several RNA viruses but not the DNA virus insect iridovirus VI (31), which replicates in the nucleus so likely does not require autophagy (32). An investigation of heritability and interpopulation differences in *D. melanogaster* lipid profiles found that *Wolbachia* abundance correlated with a gain of odd-chained fatty acids in females and an increase in phosphatidylserines, a class of phospholipids which are responsible for signaling that results in the clearing of apoptotic cells, which the authors suggested could arise from the induction of stress and apoptosis by *Wolbachia* (33). No such data are available for *Wolbachia* in mosquitoes. In order to broadly identify candidate lipid classes and lipid pathways modulated in *Wolbachia*-host metabolic interactions, an untargeted lipidomics analysis was performed on *Aedes albopictus* Aa23 cell lines containing the *wMel* or *wMelPop* strains in comparison with *Wolbachia*-free Aa23-T cells. *A. albopictus* is an invasive mosquito species (34) that is important in the transmission of DENV and chikungunya virus (CHIKV), both of which impose high and increasing global disease burdens (35, 36), but neither virus was transmitted when the naturally occurring *wAlbA* and *wAlbB* *Wolbachia* strains were replaced with *wMel* from *Drosophila melanogaster* (7, 8).

For this purpose, we used high-resolution Fourier transform ion cyclotron resonance (FT-ICR)-based nontargeted lipidomics applying both liquid chromatography-mass spectrometry (LC-MS) and nano-electrospray direct infusion mass spectrometry (DIMS). While the lipid LC-MS approach is inherently suited to reduce ion suppression and enable more rigorous annotation of *m/z* signals due to retention time information (37), the DIMS method can detect species outside the optimal range of the LC gradient, reduces ion suppression by using nano-electrospray ionization, and maximizes sensitivity and mass accuracy by acquiring data in a series of selected ion monitoring windows (38, 39).

## MATERIALS AND METHODS

***Aedes albopictus* cell lines and *Wolbachia* density analysis.** The Aa23 mosquito cell line (40), derived from *A. albopictus* eggs and cured of its native *Wolbachia* infection using antibiotics (Aa23-T), and two derived lines that we had transfected with *Wolbachia* strains from *Drosophila* to create Aa23.*wMel* and Aa23.*wMelPop* (41) were grown in 25-cm<sup>2</sup> or 75-cm<sup>2</sup> flasks kept at 27°C in Schneider's medium (Promo-Cell) with 10% fetal bovine serum (FBS) and 1% penicillin-streptomycin (Gibco). The standard passage time was 5 to 7 days. *Wolbachia* density was analyzed by quantitative real-time PCR (qPCR) via absolute quantification against a dilution curve of a vector containing single copies of the homothorax (HTH) gene (42) and *Wolbachia* surface protein (*wsp*). Primer sequences were as follows: Mos qHTH F, 5'-TGGTCTATATTGGCGAGCTA-3'; Mos qHTH R, 5'-TCGTTTTTGAAGAAGGTCA-3'; qWSP all-F, 5'-ATCTTTTAGCTGGTGGTGGT-3' (3); qWSP all-R, 5'-AAAGTCCCTCAACATCAACCC-3'.

DNA was extracted with CTAB (cetyltrimethylammonium bromide) buffer as previously described (41), 100 ng was added to a 10- $\mu$ l qPCR mixture using SYBR green Express qPCR supermix universal (Life Technologies) per the manufacturer's instruction, and qPCR was performed in an MJ Research PTC-200 DNA Engine using a Chromo4 detection system and Opticon Monitor software v3.1 (Bio-Rad Laboratories). Cycling conditions were 95°C for 4 min, followed by 40 cycles at 95°C for 15 s and then 59°C for 30 s. The number of *Wolbachia* genomes per host genome was

determined from a linear model fitted to the known plasmid standard curve values as previously described (41).

**Lipid extraction from Aa23 cell lines.** Aa23-T, Aa23.*wMel*, and Aa23.*wMelPop* cells were grown in 25-cm<sup>2</sup> flasks in 5 ml of medium with the passage of 1 ml to 5 ml of new medium every 5 days. Eight flasks per line were independently passaged for at least 5 weeks before lipid and DNA extraction. Cells were quenched 72 h after the final passage; fetal bovine serum (FBS) from the same batch was used throughout, and cell growth was monitored to ensure that cells were harvested in the late logarithmic phase at 80 to 90% confluence. A 1.6-ml volume of quenching solution (60:40, high-performance LC [HPLC]-grade methanol-water [MeOH-H<sub>2</sub>O; Sigma-Aldrich]) per flask was precooled in each 2-ml tube on dry ice to approximately -40°C. Cells were scraped into the flask medium with minimum disruption, and the cell suspension was transferred to a 15-ml tube for centrifugation at room temperature for 5 min at 1,000 relative centrifugal force (RCF). A 500- $\mu$ l cell suspension was then retained for DNA extraction. The supernatant was removed by pouring, and cell pellets were resuspended in residual medium by gentle pipetting. A 200- $\mu$ l volume of this cell suspension was added to 1.6 ml of quenching solution at -40°C and mixed immediately by inversion. Samples were centrifuged in the prechilled rotor at -9°C and 2,500 RCF for 5 min. A maximum of 10 samples were processed at a time to ensure that all were kept below 0°C. The quenching solution was removed with a glass Pasteur pipette, and the tube was weighed to estimate cell mass before being frozen at -80°C and was retained at this temperature until extraction.

For lipid extraction, HPLC-grade MeOH (EMD Millipore), H<sub>2</sub>O, and chloroform (Sigma-Aldrich) were cooled on ice, and 8  $\mu$ l of MeOH/mg pellet mass and 7.2  $\mu$ l of H<sub>2</sub>O/mg were added to each sample tube. Tubes were vortexed for 30 s and returned to ice. An 8- $\mu$ l/mg concentration of chloroform was added to 1.8-ml glass vials, and after pulse vortexing, the pellet and MeOH-H<sub>2</sub>O mixture were transferred using a glass Pasteur pipette. Samples were vortexed and incubated on ice for 10 min before centrifugation at 1,500 RCF for 15 min at 4°C. Biphasic samples were left at room temperature for 5 min before the upper layer containing polar metabolites was removed using a Hamilton syringe. A 270- $\mu$ l volume of nonpolar lipid-containing lower layer was then transferred to a 1.8-ml glass tube and stored overnight at -80°C. Seven Aa23-T samples and six samples from each infected line were used. Forty microliters of each sample was removed, and these samples were pooled to form a quality control (QC) sample before all samples were dried under nitrogen, taken back up in 270  $\mu$ l chloroform, and stored at -80°C until analysis.

**DI FT-ICR MS and data processing.** Negative-ion-mode direct-infusion (DI) FT-ICR MS was conducted using a hybrid 7-T linear ion trap FT-ICR mass spectrometer (LTQ FT Ultra; Thermo Fisher Scientific) equipped with an Advion Triversa chip-based direct-injection nano-electrospray ion source (Advion Biosciences). Samples were diluted 1:4 in 5 mM ammonium acetate (from a 1 M stock in methanol) in methanol-chloroform (3:1). Technical triplicates were run in controlled randomized order. Data were acquired from *m/z* 120 to 1,200 in 12 wide SIM (selected ion monitoring) windows (43). Additional compound identification (direct infusion tandem MS [DI-MS/MS] and multiple-stage MS [MS<sup>n</sup>]) was performed on the same instrument.

Data processing was performed using NBAF-B in-house scripts in MatLab, the SIMStitch pipeline (44). During "replicate filtering," peaks were retained if they were found in two out of three technical replicates. Subsequently a "blank filter" required that biological signals be two times the intensity of background signals to be retained. Sample filtering with a 2-ppm mass error and a 75% filter resulted in a matrix containing 2,044 peaks (*m/z* values). Normalization was performed using the probabilistic quotient normalization (PQN) method, and missing values were imputed in the resulting data matrix using the *k*-nearest neighbors (KNN) algorithm. A generalized logarithm-transformed version of this normalized, missing value-imputed matrix was generated (based on the technical variance of the QC samples) for use only in the multivariate statistical analysis.

**LC FT-ICR MS and data processing.** Reversed-phase high-performance liquid chromatography (RPLC) FT-ICR MS-based analysis of the lipids was carried out on a Thermo Scientific Dionex Ultimate 3000 system connected to the same mass spectrometer as described above. Samples were dried, and each was taken up in the original volume of solvent A (5 mM ammonium acetate, 5% isopropanol in water)-solvent B (5 mM ammonium acetate, 5% isopropanol, 5% water in acetonitrile) (1:1) and centrifuged for 10 min at 4°C and 4,000 RCF. Eight microliters of each sample was injected onto a Dionex Acclaim C<sub>30</sub> column (Thermo Scientific; 2.1 by 150 mm, 3- $\mu$ m particles) and separated at 40°C with a flow rate of 200  $\mu$ l/min and a gradient from 100% solvent A to 100% solvent B to 100% solvent C (5 mM ammonium acetate, 5% water in isopropanol) (see Table S11 in the supplemental material). The gradient was designed to thoroughly wash out polar compounds before lipid analysis. One LC FT-ICR MS analysis was performed per sample. Data were acquired in negative-ion mode from *m/z* 120 to 1,200 at a nominal resolution of 50,000 in centroid mode. A QC sample was pooled from all biological samples and analyzed repeatedly at the start and end of and equidistantly throughout the sequence. Two further QC sample runs were performed using data-dependent acquisition (MS/MS) of the most intense ions in the negative- and positive-ion modes, respectively.

RPLC FT-ICR MS lipidomics data were initially converted into netcdf (.cdf) format using Xcalibur 2.1 and processed using an R-based XCMS/Camera script (see Table S12 in the supplemental material) (45, 46) to generate an intensity matrix with a list of peak retention times. The intensity matrix was imported into the SIMStitch pipeline immediately after the replicate filter and hence included blank filtering, sample filtering, PQN normalization, KNN missing-value imputation, and the generalized logarithm transformation, as for DIMS processing above. The sample filter was set to 75%, since no technical replicate filtering was applied.

**Statistical analysis and identification of metabolites.** Principal-component analysis (PCA) was used initially to assess the overall metabolic differences between the sample groups in an unbiased manner, using the PLS\_Toolbox (version 7.8.2; Eigenvektor Research, Manson, WA, USA) within Matlab (version 8.1; The MathWorks, Natick, MA, USA). Supervised multivariate analyses were performed using partial least-squares discriminant analysis (PLS-DA) using the PLS Toolbox, with internal cross validation (venetian blinds) and permutation testing (1,000 tests each) using an in-house Matlab script, which created a single variable importance list from the latent variable (LV) vectors and forward selected these variables for an optimized PLS model. Univariate statistical analyses were used to confirm the significance of changes in individual mass spectral signals. Specifically, analysis of variance (ANOVA) was conducted using an in-house Matlab script with a false discovery rate of 5% to correct for multiple hypothesis testing (47).

For both lipid data sets, peaks were annotated and putative empirical formulae were calculated using MI-Pack software (48), with searches of the KEGG (<http://www.genome.jp/kegg/>) and Lipid Maps (<http://www.lipidmaps.org/>) databases (49–51). Additional MS/MS data were acquired as described above and analyzed in Xcalibur 3.0.63 (Thermo Fisher Scientific). Lipid classes were identified, with initial focus on the most intense species, by analysis of collected MS/MS data, isotopic patterns, and, for LC-MS, the expected relative retention times.

The data set is available in the MetaboLights database at <http://www.ebi.ac.uk/metabolights/MTBLS210>, and the R code used to generate the figures is available at <https://github.com/jcmolloy/lipidomicspaper>.

## RESULTS

Both DIMS and LC-MS were conducted on lipid extracts from Aa23-T (*Wolbachia*-uninfected), Aa23.wMel, and Aa23.wMelPop (wMel-infected and wMelPop-infected, respectively) cells. Negative-ion DIMS analysis of the lipid extracts resulted in 2,044 peaks, which clustered into distinct lipid profiles for the three groups, distinguished by PCA and PLS-DA. There were clear separations of Aa23-T and Aa23.wMel along principal component 1 (PC1)

and between Aa23-T and Aa23.wMelPop along the same axis but to a lesser degree (Fig. 1A). PLS-DA results showed that Aa23.wMelPop was separated from the other lines along latent variable 1 (LV1), while separation between Aa23-T and Aa23.wMel was mostly along LV2 and, to a lesser extent, LV1 (Fig. 1B). Internal cross validation testing of the PLS-DA model showed reasonable classification errors and significant *P* values for all three treatment groups in the PLS-DA model (see Table S1 in the supplemental material).

Differences were most profound between Aa23-T and Aa23.wMel, which was unexpected, as wMel infections are typically maintained at a lower density than wMelPop infections. However, densities can fluctuate in cell lines (52), and qPCR of DNA samples taken from six separate culture flasks per line concurrently with the lipid extraction revealed that at the time of sampling, the mean *Wolbachia* density was >3-fold higher in Aa23.wMel than in Aa23.wMelPop. The recorded densities of  $1,147 \pm 236$  wMel genomes per cell versus  $336 \pm 127$  wMelPop genomes per cell (Fig. 2) are in line with DENV-blocking densities in cell lines reported previously (53). An LC-MS analysis was performed to complement the nano-electrospray DIMS measurements. Analysis of 4,736 signals supported the pattern of separation along the principal components and latent variables observed in the analysis of the DIMS data but showed clearer segregation of the *Wolbachia*-infected and -uninfected cell lines (Fig. 3; see Table S2 in the supplemental material). Further analysis was thus undertaken focusing mostly on the LC-MS data set, which contained 2,794 signals that differed significantly in intensity between cell lines (ANOVA, *q* < 0.05) while the DIMS data set contained 513.

For both data sets, PLS-DA was also performed comparing each set of two groups, and after reclassification of the Aa23.wMel and Aa23.wMelPop groups into one “infected” group. All of the PLS-DA models had *P* values of <5% (from permutation testing) and classification errors of <20% (from internal cross validation; see Tables S3 to S10 in the supplemental material), with the DIMS model comparing Aa23-T and Aa23.wMelPop (see Table S5) being weaker than the others.

The 513 differentially regulated DIMS signals resulted in 290 putative annotations (see Table S15 in the supplemental material), and the 2,794 in the LC-MS data set resulted in 1,003 putative annotations (see Table S16) by use of the MI-Pack (48) and both the Lipid Maps and KEGG databases. This analysis clearly revealed which lipid classes differed between the three groups of samples. Additional species were annotated manually, especially nonstandard adducts [NO<sub>3</sub><sup>-</sup> and Na(OAc)<sub>2</sub><sup>-</sup>, where OAc is acetate], and others were manually curated, taking into account the measured MS/MS data, relative signal intensities, and in the case of LC-MS, retention times. For the majority of species, no MS/MS data were collected, with the larger lipids annotated by summing up their constituent acyl and alkyl chains [e.g., Cer(d18:1/18:0) is represented as Cer 36:1].

**Sphingolipids.** Many of the more intense signals in the spectra are derived from sphingolipids, which play a major structural role in plasma membranes in addition to being involved in signaling and a range of other functions within the cell (54–57). However, there has been little reported research on the biological role of specific sphingolipids in mosquitoes. Ceramides appear to be the sphingolipid class most affected by *Wolbachia* infection (Fig. 4). For example, in the LC-MS PLS-DA model comparing Aa23-T and Aa23.wMel cell lines, six different ceramides were featured in

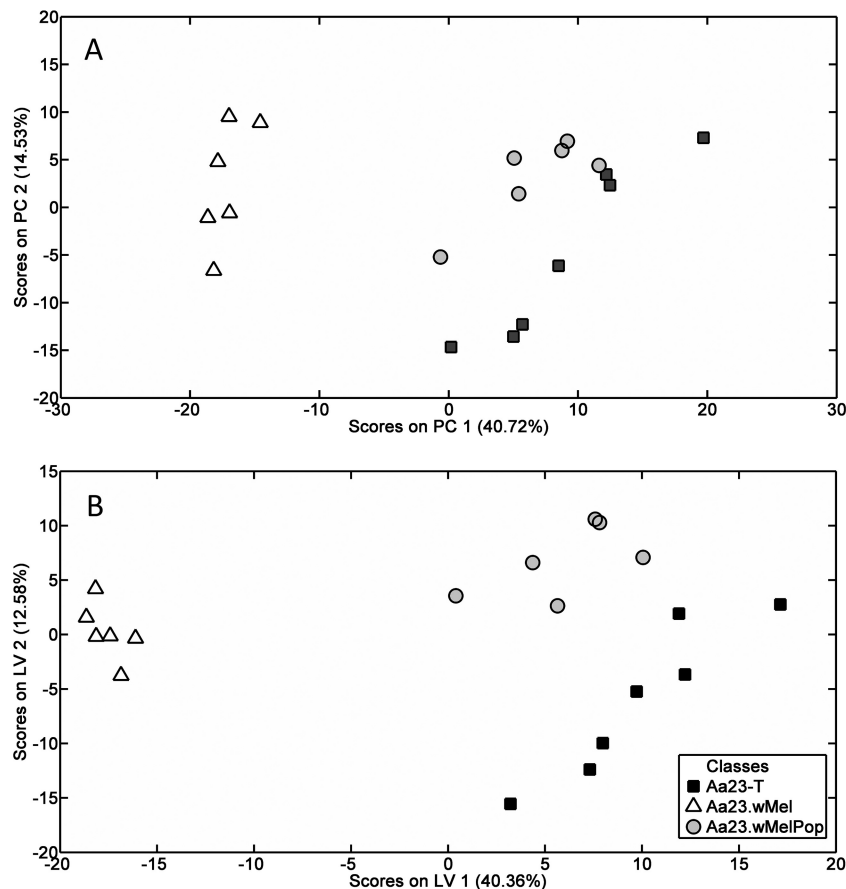


**FIG 1** Direct infusion mass spectrometry (DIMS) shows distinct lipid profiles in *Wolbachia*-infected versus uninfected *A. albopictus* Aa23 cell lines. (A) Principal-component analysis (PCA) plot showing segregation of total lipid profiles measured using DIMS. (B) Partial least-squares discriminant analysis (PLS-DA) of DIMS data. Data points represent six or seven biological replicates from Aa23-T, Aa23.wMel, and Aa23.wMelPop cell lines, and 2,044 signals from the negative-ion DIMS analysis were analyzed.

the top 10 annotated lipid signals ranked by variable importance (a vector calculated from the model's latent variables) (see Materials and Methods and the supplemental material), with an additional two  $^{13}\text{C}$  isotopic ceramide signals. Four of these ceramides also were featured in the top 10 most important ranked lipid signals for Aa23-T versus Aa23.wMelPop and for control versus infected (combined Aa23.wMel and Aa23.wMelPop).

In the DIMS data set, 80 signals were initially annotated as ceramides by MI-Pack (as the adducts  $[\text{M}-\text{H}]^-$ ,  $[\text{M}+\text{OAc}]^-$ ,  $[\text{M}+\text{Cl}]^-$ ,  $[\text{M}+^{37}\text{Cl}]^-$ , and  $[\text{M}+\text{K}-2\text{H}]^-$ , not counting further isotopic signals). Two further lipid ion series ( $[\text{M}+\text{NO}_3]^-$  and  $[\text{M}+\text{Na}(\text{OAc})_2]^-$ ) were deduced to occur from the same or similar ceramide species. Fifty-eight of these signals displayed significant differences in either direction across the three cell lines (ANOVA,  $q < 0.05$ ). In the LC-MS data set, no additional  $\text{NO}_3^-$  adducts were observed but instead multiply charged species at low  $m/z$  values corresponding to the more intense singly charged ions.

Based on the LC-MS data set, the overall mean decrease across ceramides relative to uninfected cells was 62% in Aa23.wMel and 20% in Aa23.wMelPop (Fig. 4), although some ceramide species were decreased by as much as 90% in Aa23.wMel, e.g., Cer 41:1 (Lipid Maps match d18:1/23:0) (see Fig. S17 in the supplemental material). Similar patterns emerged in both the DIMS and LC-MS data for Aa23.wMel, as all significantly altered ceramide species

decreased (see Fig. S17). Ceramide signals in Aa23.wMelPop were inconsistent in their direction of change compared to those in Aa23-T. Changes in two ceramide species, Cer 34:0 and Cer 36:0, were classed as insignificant by the ANOVA but ranked very highly in the LC-MS PLS-DA models and therefore need to be considered. Based on MS/MS data, they were putatively identified as Cer (d14:0/20:0) and Cer (d16:0/20:0) in accordance with the mechanism proposed by Hsu and Turk (see Fig. S13 and S14 in the supplemental material) (54).

Ceramide is often converted to more complex forms, e.g., by glycosylation. Glucosylceramide (GlcCer) is known to be a precursor of much more complex glycosphingolipids, although its own role in insects is undefined. In *D. melanogaster*, it is posited that GlcCer synthesis operates to reduce the ceramide levels and thus lower the apoptosis risk. Other neutral glycosphingolipids containing different monosaccharide headgroups, such as galactosylceramide (GalCer), are primarily found in brain and nervous system tissues in mammals, but little information is available on potential roles in insects. Both lipid classes were detected, but it was here not possible to positively distinguish between GalCer and GlcCer species with the same molecular mass; therefore, they are grouped as monohexosylceramides (HexCers) (Table 1). Among the  $[\text{M}+\text{H}]^-$  and  $[\text{M}+\text{OAc}]^-$  ions, 16 out of 17 and 10 out of 12, respectively, demonstrated significant changes (ANOVA,  $q <$

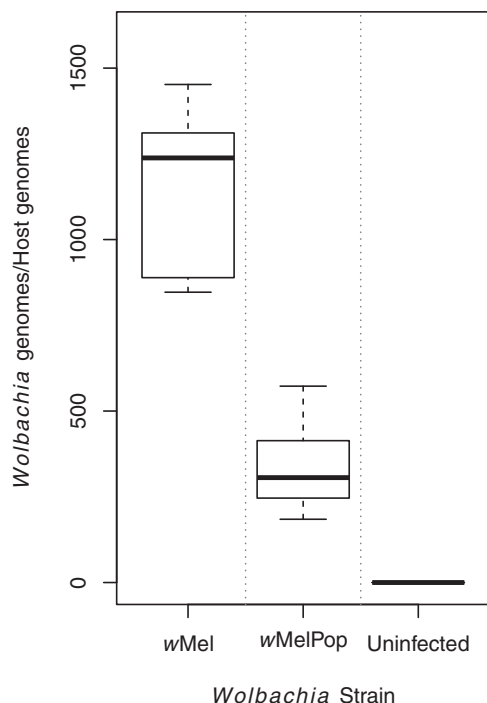


**FIG 2** *Wolbachia* density in Aa23.wMel was over three times higher than that in Aa23.wMelPop cell line. The ratios of *Wolbachia* genome copies to *A. albopictus* genome copies detected in Aa23.wMel and Aa23.wMelPop cell lines are shown. Genome copies were determined by absolute quantification using a standard curve of plasmid DNA containing the genes of interest. Results are from eight replicates per cell line, independently passed for 5 weeks, with two replicates of uninfected Aa23 used as a negative control.

0.05). In Aa23.wMel, all HexCer species decreased by a mean of 32%, while in Aa23.wMelPop, both decreases and increases were observed (average increase of 5%). As for ceramides, the highest increases in Aa23.wMelPop were observed for saturated species (HexCer 34:0 and 36:0). Less clear patterns were observed in the remaining species, although they seemed to follow a pattern similar to that of the simple ceramides.

Lactosylceramides (LacCer) were also detected in the LC-MS data set, with 9 of 14 species showing significant alterations in *Wolbachia*-infected cells. Longer-chain LacCer species were decreased in both Aa23.wMel and Aa23.wMelPop; e.g., LacCer 40:1 (annotated by MI-Pack as d18:1/22:0) was reduced by 81% in Aa23.wMel and 51% in Aa23.wMelPop. However, species with shorter fatty acid chains (LacCer 34:1 and 36:1) were increased in Aa23.wMel by 1.52- to 1.90-fold and showed limited changes in Aa23.wMelPop.

The clear trend across most ceramides was for depletion in the presence of higher-density *Wolbachia* infections (Fig. 4; see Fig. S17 in the supplemental material). This was also reflected in levels of sphingomyelin (SM), which consists of a ceramide with a phosphorylcholine (PC) headgroup. SM is not synthesized by dipterans (55) but in cell culture could potentially be incorporated from lipoproteins in FBS. Dipterans *de novo* synthesize phosphatidylethanolamine ceramides (PE-Cer), a structural analogue of SM with a phosphatidylethanolamine (PE) instead of a PC headgroup, which functionally replaces SM in insect plasma membranes but imparts different membrane properties (16).

Of several automatically annotated SM  $[M-H]^-$  and  $[M+OAc]^-$

signals, the former series could be identified as 15 likely PE-Cer species (see Table S2 in the supplemental material), and it is possible that more signals represent PE-Cer. All were significantly decreased in Aa23.wMel compared to Aa23-T, with the largest decreases in PE-Cer 42:1, 42:2, 40:1, and 39:1. Similarly, 15 of 16 PE-Cer species decreased in Aa23.wMelPop, but PE-Cer 34:0 (+2% increase) and another saturated species, PE-Cer 36:0, were among the least changed. This pattern clearly followed that seen in ceramides (see Fig. S17), although in this case, no strongly increasing signals were seen. Of the 10 remaining species annotated as SM, seven were significantly differentially regulated in *Wolbachia*-infected lines. The mean decrease across sphingomyelin species in Aa23.wMel was 35% (Fig. 4), while Aa23.wMelPop saw a 28% increase. All but one species (SM 42:3) were downregulated in the more densely wMel-infected line, especially two saturated species (SM 38:0 and 34:0). However, in Aa23.wMelPop, five species were upregulated without a clearly recognizable pattern. There is no obvious correlation with chain size or saturation.

One shared pattern between Cer, HexCer, PE-Cer, and SM was the extreme difference in the change of the 34:0 species, strongly decreased in Aa23.wMel and strongly increased in Aa23.wMelPop, making Cer 34:0 the most important species in both the control versus infection model and the Aa23.wMel versus Aa23.wMelPop PLS-DA model. The biological relevance of this is unclear.

Not all precursors of sphingolipid pathways, such as sphingosine, were detected by either DIMS or LC-MS, but an overall picture of the sphingolipid metabolic network was nevertheless obtained (Fig. 5). For example, 15 of the 17 ceramide signals which showed no significant overall change or showed a small reduction only in the Aa23.wMel line were, according to the Lipid Maps database matches, dihydroceramides, an intermediate in the *de novo* synthesis pathway. There is insufficient information to determine if this is because metabolic flux is concentrated on other pathways and therefore the dihydroceramide pool is being retained or if the dihydroceramide pool is actively utilized as a source of ceramide but an intervening rate-limiting step still results in overall ceramide reduction.

**Diglycerides.** Few single-chain fatty acids (monoacylglycerols [MGs]) were included in the data sets, so a general analysis is not possible. Diacylglycerols (DGs) were abundant in the LC-MS data set but less so in the DIMS data set. DGs are involved in secondary signaling and are major components of lipid droplets alongside triglycerides (TGs), which were not analyzed here. In the LC-MS data set, 29 DG species remain after the removal of minor ion forms and isotopes, consisting of  $[M+OAc]^-$  and  $[M+Cl]^-$  series. Most of these are significantly changed according to the ANOVA ( $q < 0.05$ ), i.e., 15 out of 23 and 5 out of 6, respectively. Both Aa23.wMel and Aa23.wMelPop show decreases and increases in DG species abundance compared to Aa23-T across the class (Fig. 6), but with an average decrease of 32% for Aa23.wMel and an average increase of 17% for Aa23.wMelPop. The pattern of change by saturation and carbon chain length (see Fig. S18 in the supplemental material) is more similar to that observed for ceramides (see Fig. S17) in Aa23.wMel than in Aa23.wMelPop.

Interestingly, in this LC-MS data set, the only lipid in the top 25 signals ranked by variable importance in all the PLS-DA models that was not a sphingolipid or phospholipid was DG(16:0/18:1) ( $[M+OAc]^-$ ) or an isomer, which is reduced by 65% in Aa23.wMel but increased by 42% in Aa23.wMelPop. The changes

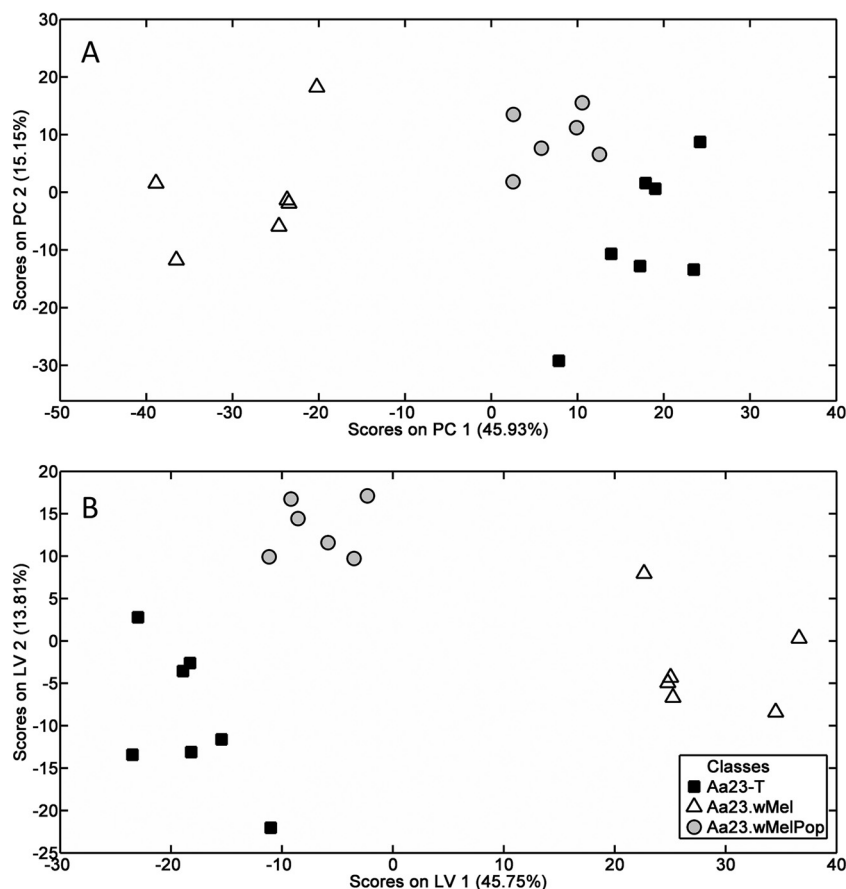


FIG 3 Liquid chromatography-mass spectrometry (LC-MS) shows distinct lipid profiles in *Wolbachia*-infected versus uninfected *A. albopictus* Aa23 cell lines. (A) Principal-component analysis (PCA) plot showing segregation of total lipid profile derived from LC-MS. (B) Partial least-squares discriminant analysis (PLS-DA) of resulting data. Points represent six or seven biological replicates from Aa23, Aa23.wMel, and Aa23.wMelPop cell lines, and 4,736 signals from the LC-MS analysis were analyzed.

of the  $[M+Cl]^-$  form follow the same directions but are less extreme. Overall, the significance of the changes and distribution is unclear. A previous report correlated increased odd-chain fatty acids with *Wolbachia* infection (33); the few DG species observed here that clearly contain odd chains (DG 29:1, 31:1, and 31:2) show mostly intensity increases. In addition, the interpretation of the *D. melanogaster* data was based on its lack of capacity to synthesize odd-chain fatty acids, which would therefore be supplied by symbionts or gut microflora. This interpretation does not hold in cell cultures, as the medium is supplemented with mammalian-derived serum (FBS), which contains odd-chained FAs and therefore will confound or mask a potential effect of *Wolbachia* infection.

**Other phospholipids.** Phospholipids carry out a wide range of functions in the cell; most critically, they are able to form lipid bilayers and are therefore required in the plasma membrane, but many also participate in signaling. Phosphatidylethanolamines (PEs) and phosphatidylcholines (PCs) are the primary components of cellular membranes in *D. melanogaster* and have previously been found in high abundance in mosquitoes (16). PCs are cylindrically shaped and spontaneously form lipid bilayers, while PEs are cone shaped and thought to help control membrane curvature and to increase membrane fluidity. PCs provide the head-group for SM and PEs for Cer-PE. Phosphatidylserine (PS) species

are thought to be important for recognizing and removing apoptotic cells. A range of differences in abundance was found across the *Wolbachia*-infected cell lines (Fig. 7).

PS, PCs, and PEs cannot be clearly distinguished by simple mass spectrometry alone, as PE species are isobaric with PC species and acetate adducts of PC species are isobaric with deprotonated PS species. They can be distinguished based on intensity profiles, retention times, and MS/MS profiles, but here we focus on manually curated annotations (see Tables S15 and S16 in the supplemental material) among the 272 species annotated by MI-Pack as PC, PE, PS, or their diacyl- or lysoforms in the LC-MS data set. The DIMS data set contains 136 PC, PE, and PS signals, but there are a number of mixed species and these are more challenging to assign than LC-MS signals, for which isobaric PE and PC species are unlikely to have the same retention time. Similar considerations also hold true for annotations of phosphatidylinositols (PIs) and phosphatidylglycerols (PGs), so the following analysis concentrates on LC-MS data.

Forty-four out of 53 (diacyl) PC signals were identified with significant differential regulation in *Wolbachia*-infected lines. There was an overall decrease of 38% in Aa23.wMel species and just 4% in Aa23.wMelPop species (Fig. 7), but the picture by species was more complicated, with the vast majority showing up to an 80% decrease in Aa23.wMel but seeming inconsistency in

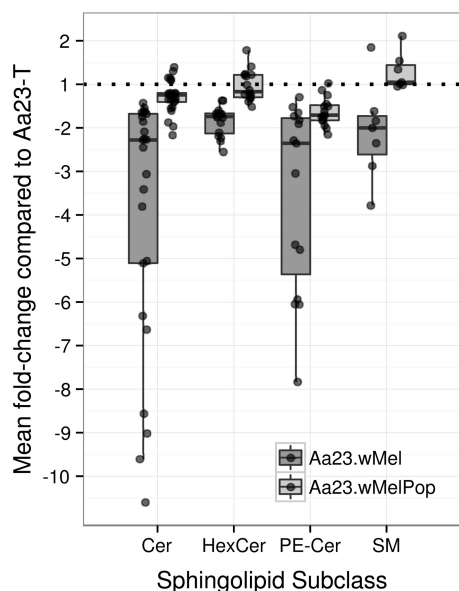


**FIG 4** Sphingolipids show a mean decrease in *Wolbachia*-infected *A. albopictus* Aa2 cell lines. A box plot shows mean fold changes in sphingolipid species abundance in the *Wolbachia*-infected *A. albopictus* cell lines Aa23.wMel and Aa23.wMelPop relative to that of uninfected Aa23-T. Negative fold changes reflect the increase of the signal in the uninfected cells compared to that of the infected cells. LacCer is not included due to the small number of data points for this lipid class. Cer, ceramide, [M+OAc]<sup>-</sup> ion series; HexCer, hexosylceramide, [M-H]<sup>-</sup> ion series; PE-Cer, phosphatidylethanolamine ceramide, [M-H]<sup>-</sup> ion series; SM, sphingomyelin, [M+OAc]<sup>-</sup> ion series.

Aa23.wMelPop (see Fig. S19). In the DIMS data set, only 13 significantly changed [M+OAc]<sup>-</sup> ions could be annotated with some certainty, but they also showed two clear trends: a decrease of longer-chain PCs and an increase of shorter-chains in the infected cells, which were exaggerated in Aa23.wMelPop and Aa23.wMel, respectively.

For lyso-PCs (LPCs), 7 of 11 decrease in Aa23.wMel, i.e., from unsaturated LPC 18:1 and 16:1 by around 80% to saturated LPC 14:0 by 52% and LPC 16:0 by 30%. In Aa23.wMelPop, LPC 18:1 and 17:1 show the largest decrease, but LPC 16:0, the least decreased species in Aa23.wMel, is the only increased LPC in both the LC-MS and DIMS data sets. The overall decrease in PC levels parallels the trend for a greater decrease of saturated lipids seen for sphingolipid depletion in Aa23.wMel, while again trends are less clear for Aa23.wMelPop.

PS species are important for recognizing and removing apoptotic cells. No PS species was featured in the top 100 signals (ranked by variable importance) for either *Wolbachia* cell line infection, and most of the 147 species initially designated putative PS by automatic annotation are likely PC adducts. Just 8 of the remaining 12 show a significant change, of which 7 increase in both cell lines.

For lyso-PEs (LPEs), only two of nine were significantly changed: LPE 16:0 increased and LPE 20:0 decreased in both infected cell lines, although LPE 20:1 also decreased significantly according to the DIMS data set. In contrast, 61 of 81 (75%) of diacyl-PEs (PEs) showed differential regulation in the LC-MS data (see Fig. S20 in the supplemental material). Differences between Aa23-T and Aa23.wMel were clear and followed a trend in abundance that was much more conserved across Aa23.wMel and

Aa23.wMelPop than in the PCs presented above (see Fig. S20). The PE class has the most intense ions in the spectra (see Fig. S21) and includes some multiply charged ion forms, which facilitates their interpretation. Despite the large changes for some species, the average change for both infected cell lines was just a 2% increase (Fig. 7). Only a few multiunsaturated PE species could be rigorously annotated in the DIMS data set. For these limited data, we again see in both cell lines that fold changes depend on molecular weight and there is an overall intensity increase.

Phosphatidylinositol lipids (PIs) induce the PI 3-kinase (PI3K) pathway, which plays an essential role in cell survival and growth. Among 59 PI signals, 30 were significantly changed in the ANOVA ( $q < 0.05$ ), with the largest mean increase of any lipid class considered at 94% in Aa23.wMel and 27% in Aa23.wMelPop. Only four of these 30 decreased in Aa23.wMel (PI 44:7, 40:8, 38:4, and 35:2) but with no clear trend in chain length or saturation, although the most reduced of these were also two of the three longest species. Patterns were more visible in data from Aa23.wMelPop, where the 11 decreasing signals contained (with the exception of PI 32:2) three to eight double bonds and the 11 most increased species (>40%) contained zero to two double bonds (with the exception of PI 36:5), including all six saturated species.

Phosphatidylglycerols (PG), the lipid class with the second most intense ions in the spectra, were also mostly elevated across the 40 significantly changed signals in this class (mean percent change without multiply charged ions: for Aa23.wMel, 50% increase; for Aa23.wMelPop, 17% increase), similar to PIs. As was typical across all lipid classes, changes were usually in the same direction in both Aa23.wMel and wMelPop, with larger effect sizes

**TABLE 1** Count of changes in annotated lipid classes in the LC-MS data set<sup>a</sup>

Lipid class <sup>b</sup>	No. of changes in lipid class (wMel/wMelPop) <sup>c</sup>				
	-/-	+ +	-/+	+/-	None
<b>Sphingolipids</b>					
Ceramide	42	0	11	0	4
HexCer	15	0	11	0	3
LacCer	4	2	0	3	5
SM	2	1	6	0	3
PE-Cer	14	0	1	0	0
<b>Other phospholipids</b>					
PC	21	5	15	0	9
PE	33	26	0	0	13
PS	2	5	0	0	4
PI	4	21	0	8	19
PG	8	18	5	5	16
<b>Diglycerides</b>					
	6	4	10	0	10

<sup>a</sup> Data indicate direction of statistically significant changes in the abundance of lipid classes for Aa23.wMel and Aa23.wMelPop, respectively (ANOVA,  $q < 0.05$ ). Counts represent signals, some of which are different ion forms of the same lipid species (singly charged ions only).

<sup>b</sup> HexCer, monohexosylceramides; LacCer, lactosylceramide; SM, sphingomyelin; PE-Cer, phosphatidylethanolamine ceramide; PC, phosphatidylcholine; PE, phosphatidylethanolamine; PS, phosphatidylserine; PI, phosphatidylinositol; PG, phosphatidylglycerol; DG, diacylglycerol (PC, PE, PS, PI, and PG are diacyl species).

<sup>c</sup> -/-, downregulated for both wMel and wMelPop; +|+, upregulated for both; -/+, downregulated for wMel and upregulated for wMelPop; +/-, upregulated for wMel and downregulated for wMelPop; none, not significantly changed.

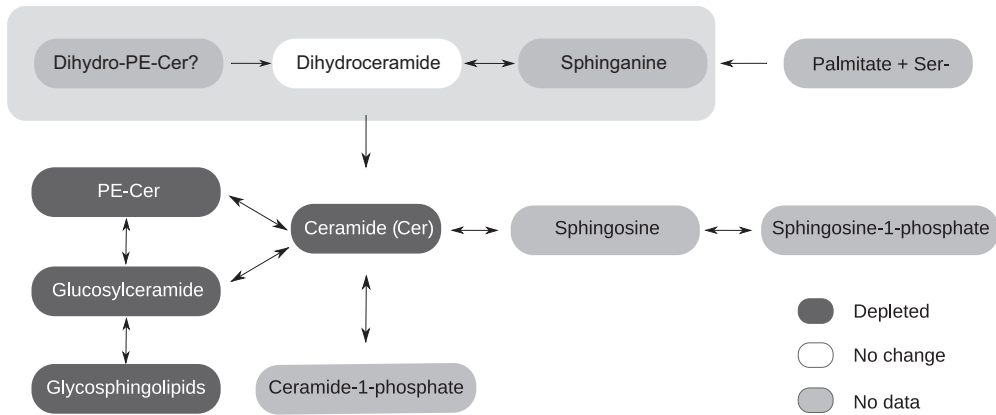


**FIG 5** The sphingolipid metabolic network is modulated in *Wolbachia*-infected *A. albopictus* Aa23 cell lines. A simplified diagram of sphingolipid metabolism (in accordance with reference 16) is shown. Ceramide is synthesized *de novo* in the endoplasmic reticulum from serine and palmitoyl-coenzyme A through the intermediary metabolites sphinganine and dihydroceramide. Ceramide is then trafficked to the Golgi apparatus, where glycosphingolipids and phosphatidylethanolamine ceramide (PE-Cer) are made and transported to the plasma membrane. In most other eukaryotes, sphingomyelin (SM) is dominant and PE-Cer is a minor lipid, but in general dipterans do not generate SM. Ceramide is broken down into sphingosine and sphingosine-1-phosphate in various intracellular compartments to be recycled or further metabolized. PE-Cer is thought to be hydrolyzed to dihydroceramide as for SM (59). Colors indicate the relative regulation of each lipid class in Aa23.wMel compared to Aa23-T, as derived from LC-MS data. Dark gray, downregulation; white, no change; light gray, no data.

in the more densely infected Aa23.wMel. The eight signals in Aa23.wMel and four in Aa23.wMelPop that were >30% lower all featured at least four double bonds, while those with >50% increases contained only one or no double bond, with two exceptions (43:3 and 36:2). It is interesting to note that in these >50% increased samples, wherever MS/MS data are available, the *m/z* 281 ion corresponding to oleic acid is very intense. The largest increases were seen in PG 36:2 and 34:1; these and PG 34:0 are also among the more important “forward selected” species in the corresponding PLS-DA models.

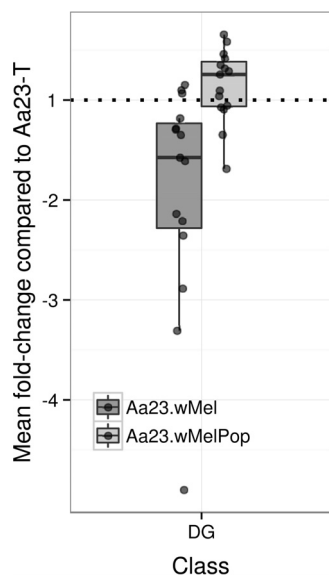


**FIG 6** Diacylglycerols (DGs) are modulated in *Wolbachia*-infected *A. albopictus* Aa23 cell lines. A box plot shows the mean fold changes (see description in the legend to Fig. 4) in DG species abundance ( $[M+OAc]^-$  ion series only) in *Wolbachia*-infected *A. albopictus* cell lines Aa23.wMel and Aa23.wMelPop relative to uninfected Aa23-T. The horizontal dotted line depicts no change.

**DISCUSSION**

We used DIMS and LC-MS to profile the lipidome of *Wolbachia*-infected *A. albopictus* cells and observed a distinct segregation between uninfected and infected cells, which was heightened at a high *Wolbachia* density. The two data sets were largely consistent in their results. High-density *Wolbachia* infection resulted in the downregulation of several sphingolipids, which as a lipid class are known to affect membrane structure, fluidity, curvature, and pro-

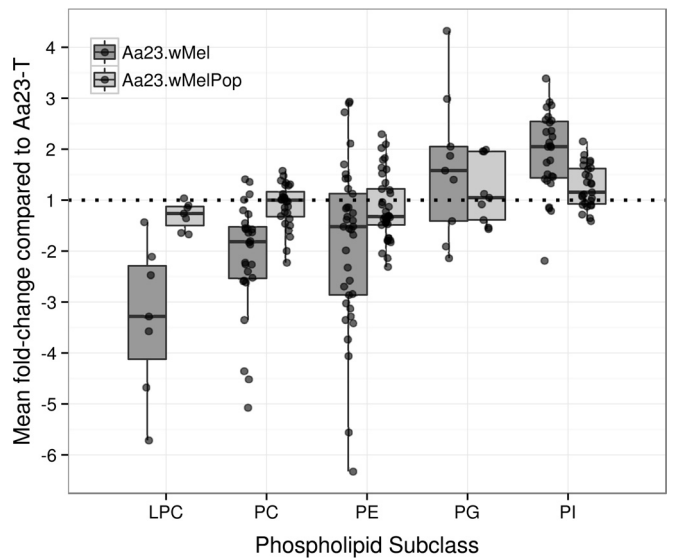


**FIG 7** Some phospholipid classes are modulated in *Wolbachia*-infected *A. albopictus* Aa23 cell lines. A box plot shows mean fold changes (see description in the legend to Fig. 4) in phospholipid species abundance across selected classes in Aa23.wMel and Aa23.wMelPop relative to Aa23-T. The horizontal dotted line depicts no change. LPC, lyso-phosphatidylcholine; PC, phosphatidylcholine (both  $[M+OAc]^-$  ion series only); PE, phosphatidylethanolamine; PG, phosphatidylglycerol; PI, phosphatidylinositol (all  $[M-H]^-$  ion series only).

tein complex assembly in lipid rafts (57). Sphingolipids and other identified lipids with significant changes, such as PCs and PIs, also function as signaling molecules and control important pathways, such as trafficking, autophagy, and apoptosis.

DG species showed a variety of responses, which overall indicates minor depletions in DG in the densely infected Aa23.wMel line. It is unclear how this relates to flux in fatty acid synthesis and degradation, because many straight-chain free fatty acids and monoacylglycerols could not be sufficiently annotated (mostly because of a high background signal, for example, due to saturated fatty acids in the solvents). This can be remedied by optimization of extraction procedures and mass spectrometry setup for this lipid class, but no clear inferences can be drawn from the current data. Little evidence has been found elsewhere for a major impact of *Wolbachia* on fatty acid metabolism; one study found a 2.36-fold increase in fatty acid synthase (FAS) mRNA expression in wMel-infected *A. aegypti* mosquitoes (15).

While other lipids were modulated and each class included at least a few species with quite noteworthy differences, the class changes in sphingolipids, PC, and PI are significant and immediately suitable for the design of downstream functional assays. In combination, the data observed suggest a substantial reprogramming of the host lipid metabolic network. However, the flux within the system and the mechanism of this modulation have yet to be elucidated. Our observations are contextualized below in relation to the current knowledge about lipids and their interactions with similar bacteria, viruses, and hosts.

**Wolbachia-host interactions and lipid metabolism.** *Wolbachia* wMel has a highly reduced genome with limited lipid metabolic capabilities (27). It only retains genes for fatty acid elongation and limited transformations of glycerolipids and glycerophospholipids. While many other obligate intracellular bacteria have the capacity to degrade but not produce sphingolipids, *Wolbachia* bacteria have neither of these gene pathways (27). This means that changes in lipid composition are unlikely to be due to the direct action of *Wolbachia* metabolic enzymes but are more likely to involve a host response to *Wolbachia* infection or manipulation of host lipid pathways by *Wolbachia*.

The changes observed in our analysis might have implications for *Wolbachia* maintenance and infectivity through alteration of structural membrane properties. Specific depletion of bioactive sphingolipids such as Cer and PE-Cer was observed in *Wolbachia*-infected *A. albopictus* mosquitoes. This finding is interesting when considered with previous evidence for cholesterol depletion in *Wolbachia*-infected mosquitoes (29) because, in contrast, sphingolipids increase in cholesterol-depleted *D. melanogaster* and are hypothesized to play an analogous and compensating structural role (58). Our lipidomics analyses revealed no findings on sterols, but future work combining sterol data with functional testing of membrane properties during *Wolbachia* infection could be revealing.

Sphingomyelin-, cholesterol-, and ceramide-depleted membranes are more fluid than enriched membranes (58, 59), and this could be advantageous for *Wolbachia* bacteria, as cellular membranes are reconfigured to provide the double membrane-bound, Golgi apparatus-derived intracellular vesicles in which they dwell (60). However, these lipids are also involved in forming lipid rafts in plasma membranes which most evidence suggests are useful for bacterial invasion and persistence (61). One possibility to explore is that sphingolipid depletion limits autophagy and apoptosis even

where *Wolbachia* is causing cellular stress. This hypothesis fits with our current knowledge that activation of autophagy can reduce *Wolbachia* bacterial density (30) and that accumulated ceramides are able to activate both autophagic and apoptotic pathways by interacting with the mTOR pathway (62, 63) and have been shown to target autophagosomes to mitochondria (63).

Phospholipid classes showed more moderate overall changes, although within each class there were clearly differentially regulated species. The clearest modulation in phospholipids was a 2-fold increase in PIs in Aa23.wMel and an overall downregulation of PCs. Due to a paucity of information on the role of specific phospholipid species in insects, the functional significance of these findings is difficult to predict. PIs play key roles in receptor-mediated signal transduction, membrane dynamics, and cell remodeling via actin and other cytoskeletal components (64). Several vacuolar pathogens are known to modulate PI levels either directly through production of PI metabolic enzymes or through manipulation of host pathways (65, 66). The *Wolbachia* genome does not encode PI-modifying enzymes, but it could manipulate or subvert host pathways and there is a precedent for a PI increase in bacterial infection. For example, *Shigella flexneri* upregulates various PI species (67) postentry, and this is thought to provide protection from apoptosis. PIs thus provide another likely candidate lipid class for involvement in the maintenance and regulation of *Wolbachia* infections.

PCs are primarily structural molecules and also play a role in the aforementioned lipid raft domains. They are expected to form a major part of intracellular bacterial membranes, but the composition of the *Wolbachia* membrane is currently unknown. Many bacterial infections appear to increase rather than deplete PCs, and several pathogenic bacteria are able to synthesize their own using host-provided choline (68), which *Wolbachia* could not as it lacks the necessary genes. The mechanism by which abundance is altered and any functional impacts on the *Wolbachia*-host relationship thus remain to be established, and there are few predictions that can be inferred from other systems in this case.

**Implications for pathogen transmission.** Host lipids are vital to the viral and bacterial life cycle; therefore, it might be expected that both *Wolbachia* bacteria and DENV would evolve the means to modulate the cellular lipidome to ensure their own preservation and replication or the means to thrive in spite of lipid-mediated host responses to infection. This expectation appears to be upheld in DENV-infected *A. albopictus* C6/36 cells, in which the cellular lipid profile was substantially altered upon infection in a way that favors viral propagation (16).

The data presented here are striking in comparison to observations on DENV infection, because the same lipid classes that are depleted in *Wolbachia*-infected *A. albopictus* Aa23 cells are selectively enriched in DENV-infected *A. albopictus* C6/36 cells (16). Sphingomyelin and ceramides were upregulated in both the whole cell and the replication complex membranes during DENV infection, including enrichment of specific ceramide species in the 16,000-molecular-weight pellet containing the replication complex. This may be a cellular response or might reflect a direct need for ceramides in the viral life cycle (16), particularly in forming negative curvature of lipid bilayers as observed in some DENV-induced membrane structures. Sphingolipids have also been shown to be important in the pathogenesis of a variety of other intracellular pathogens, including *Plasmodium* parasites, regulating host-microbe interactions (69).

In addition to generating favorable membrane properties, ceramide enrichment in DENV infection also appears to upregulate autophagy for fatty acid provision, and this is a requirement for viral replication in both mammalian and mosquito cells (16, 19, 70). Ceramide also increases apoptosis in some circumstances, but DENV infection antagonizes apoptosis pathways and is a persistent infection, so it seems unlikely that ceramide is being utilized for this purpose. As *Wolbachia* bacteria are potentially targeted by autophagy (30) and are therefore under significant selection pressure to subvert or downregulate the process, *Wolbachia* and DENV oppose each other in terms of host cell lipid regulation, which could be significant with respect to virus transmission blocking. Likewise, unsaturated PC, depleted in the presence of *Wolbachia*, was the most increased phospholipid in DENV-infected cells, perhaps due to its role in membrane curvature and maintaining fluid membranes (16), potentially aiding remodeling by viruses.

The results presented have provided new directions for research into *Wolbachia*-induced modulation of host lipid metabolism and implications for DENV infection and transmission. Some caution is needed in interpreting results, since the cell line used was derived from *A. albopictus* eggs, and further studies should examine different tissues in adult insects, such as the fat body, and in organs critical to virus transmission, i.e., midguts and salivary glands. This will be particularly informative given that although the Aa23 cell line is heterogeneous (40), its composition will not fully reflect cell differentiation in adult mosquitoes, in which certain cells such as adipocytes are known to store more fat than others. Whole-organism studies are also necessary to ascertain the lipid environments likely to be encountered by pathogens and *Wolbachia* through their natural life cycle. Lipid profiles can differ at the tissue level; for instance, the fat body is known to play a specific role in lipid storage and metabolism, meaning that both the lipid environment and distribution of microorganisms in different tissues will alter during development and the course of infections. Diet, age, and development can also be controlled in whole mosquitoes, while cell line growth and proliferation can be variable, all of which may impact lipid profiles.

Due to the different direction and not simply magnitude of some lipid alterations observed at increasing *Wolbachia* density in the Aa23 lines, the role of density and the relative impact of *Wolbachia*-induced changes in host lipid metabolism in comparison to the role of *Wolbachia* metabolism itself need to be examined. Subcellular investigation will also be informative; for example, different lipid profiles have been found in both the endoplasmic reticulum and 16,000-molecular-weight replication complex during DENV infection (16). A more detailed analysis of both lipid-bound and free fatty acids and various sterols and derivatives would be also be very useful, because this investigation did not provide sufficient data on these classes of lipids and related metabolites, which have already been linked to *Wolbachia*-host interactions (29). The multiple effects of *Wolbachia* on the cellular lipid profile mean that determining which components directly affect viral replication will not be straightforward, since it seems likely that modulation of multiple lipid species will contribute to viral inhibition. The role of sphingolipids is a priority area for future research and should add to an emerging picture of the molecular mechanisms underpinning *Wolbachia*-mosquito-virus interactions.

## ACKNOWLEDGMENTS

The study was supported by Wellcome Trust award WT095121, BBSRC award BB/H016511/1, and Natural Environment Research Council (NERC) Biomolecular Analysis Facility (NBAF) at the University of Birmingham (R8-H10-61), NBAF grant number 720.

## FUNDING INFORMATION

This work, including the efforts of Steven P. Sinkins, was funded by Wellcome Trust (WT095121). This work, including the efforts of Jennifer C. Molloy, was funded by Biotechnology and Biological Sciences Research Council (BBSRC) (BB/H016511/1). This work, including the efforts of Ulf Sommer and Mark Viant, was funded by Natural Environment Research Council (NERC) (R8-H10-61).

## REFERENCES

- Hoffmann AA, Turelli M. 1997. Cytoplasmic incompatibility in insects, p 42–80. In O'Neill S, Hoffmann AA, Werren J (ed), *Influential passengers: microorganisms and invertebrate reproduction*. Oxford University Press, Oxford, United Kingdom.
- Kambris Z, Cook PE, Phuc HK, Sinkins SP. 2009. Immune activation by life-shortening *Wolbachia* and reduced filarial competence in mosquitoes. *Science* 326:134–136. <http://dx.doi.org/10.1126/science.1177531>.
- Moreira LA, Iturbe-Ormaetxe I, Jeffery JA, Lu G, Pyke AT, Hedges LM, Rocha BM, Hall-Mendelin SS, Day A, Riegler M, Hugo LE, Johnson KN, Kay BH, McGraw EA, van den Hurk AF, Ryan PA, O'Neill SL. 2009. A *Wolbachia* symbiont in *Aedes aegypti* limits infection with dengue, chikungunya, and *Plasmodium*. *Cell* 139:1268–1278. <http://dx.doi.org/10.1016/j.cell.2009.11.042>.
- Kambris Z, Blagborough AM, Pinto SB, Blagrove MS, Godfray HC, Sinden RE, Sinkins SP. 2010. *Wolbachia* stimulates immune gene expression and inhibits *Plasmodium* development in *Anopheles gambiae*. *PLoS Pathog* 6:e1001143. <http://dx.doi.org/10.1371/journal.ppat.1001143>.
- Bian G, Xu Y, Lu P, Xie Y, Xi Z. 2010. The endosymbiotic bacterium *Wolbachia* induces resistance to dengue virus in *Aedes aegypti*. *PLoS Pathog* 6:e1000833. <http://dx.doi.org/10.1371/journal.ppat.1000833>.
- Walker T, Johnson PH, Moreira LA, Iturbe-Ormaetxe I, Frentiu FD, McMeniman CJ, Leong YS, Dong Y, Axford J, Kriesner P, Lloyd AL, Ritchie SA, O'Neill SL, Hoffmann AA. 2011. The wMel *Wolbachia* strain blocks dengue and invades caged *Aedes aegypti* populations. *Nature* 476:450–453. <http://dx.doi.org/10.1038/nature10355>.
- Blagrove MSC, Arias-Goeta CA, Failloux A, Sinkins SP. 2012. The *Wolbachia* strain wMel induces cytoplasmic incompatibility in and blocks dengue transmission by *Aedes albopictus*. *Proc Natl Acad Sci U S A* 109:255–260. <http://dx.doi.org/10.1073/pnas.1112021108>.
- Blagrove MSC, Arias-Goeta CA, Failloux A-B, Sinkins SP. 2013. *Wolbachia* wMel transinfection in *Aedes albopictus* is not detrimental to host fitness and inhibits chikungunya virus. *PLoS Negl Trop Dis* 7:e2152. <http://dx.doi.org/10.1371/journal.pntd.0002152>.
- Bian G, Joshi D, Dong Y, Lu P, Zhou G, Pan X, Xu Y, Dimopoulos G, Xi Z. 2013. *Wolbachia* invades *Anopheles stephensi* populations and induces refractoriness to *Plasmodium* infection. *Science* 340:748–751. <http://dx.doi.org/10.1126/science.1236192>.
- van den Hurk AF, Hall-Mendelin S, Pyke AT, Frentiu FD, McElroy K, Day A, Higgs S, O'Neill SL. 2012. Impact of *Wolbachia* on infection with chikungunya and yellow fever viruses in the mosquito vector *Aedes aegypti*. *PLoS Negl Trop Dis* 6:e1892. <http://dx.doi.org/10.1371/journal.pntd.0001892>.
- Hoffmann AA, Montgomery BL, Popovici J, Iturbe-Ormaetxe I, Johnson PH, Muzzi F, Greenfield M, Durkan M, Leong YS, Dong Y, Cook H, Axford J, Callahan AG, Kenny N, Omodei C, McGraw EA, Ryan PA, Ritchie SA, Turelli M, O'Neill SL. 2011. Successful establishment of *Wolbachia* in *Aedes* populations to suppress dengue transmission. *Nature* 476:454–457. <http://dx.doi.org/10.1038/nature10356>.
- Hoffmann AA, Iturbe-Ormaetxe I, Callahan AG, Phillips BL, Billington K, Axford JK, Montgomery B, Turley AP, O'Neill SL. 2014. Stability of the wMel *Wolbachia* infection following invasion into *Aedes aegypti* populations. *PLoS Negl Trop Dis* 8:e3115. <http://dx.doi.org/10.1371/journal.pntd.0003115>.
- Frentiu FD, Zakir T, Walker T, Popovici J, Pyke AT, van den Hurk A, McGraw EA, O'Neill SL. 2014. Limited dengue virus replication in field-

- collected *Aedes aegypti* mosquitoes infected with *Wolbachia*. PLoS Negl Trop Dis 8:e2688. <http://dx.doi.org/10.1371/journal.pntd.0002688>.
14. Pan X, Zhou G, Wu J, Bian G, Lu P, Raikhel AS, Xi Z. 2012. *Wolbachia* induces reactive oxygen species (ROS)-dependent activation of the Toll pathway to control dengue virus in the mosquito *Aedes aegypti*. Proc Natl Acad Sci U S A 109:E23–31. <http://dx.doi.org/10.1073/pnas.1116932108>.
  15. Rancès E, Ye YH, Woolfit M, McGraw EA, O'Neill SL. 2012. The relative importance of innate immune priming in *Wolbachia*-mediated dengue interference. PLoS Pathog 8:e1002548. <http://dx.doi.org/10.1371/journal.ppat.1002548>.
  16. Perera R, Riley C, Isaac G, Hopf-Jannasch AS, Moore RJ, Weitz KW, Pasa-Tolic L, Metz TO, Adamec J, Kuhn RJ. 2012. Dengue virus infection perturbs lipid homeostasis in infected mosquito cells. PLoS Pathog 8:e1002584. <http://dx.doi.org/10.1371/journal.ppat.1002584>.
  17. Carro AC, Damonte EB. 2013. Requirement of cholesterol in the viral envelope for dengue virus infection. Virus Res 174:78–87. <http://dx.doi.org/10.1016/j.virusres.2013.03.005>.
  18. Rothwell C, LeBreton A, Ng CY, Lim JY, Liu W, Vasudevan S, Labow M, Gu F, Gaither LA. 2009. Cholesterol biosynthesis modulation regulates dengue viral replication. Virology 389:8–19. <http://dx.doi.org/10.1016/j.virol.2009.03.025>.
  19. Heaton NS, Randall G. 2010. Dengue virus-induced autophagy regulates lipid metabolism. Cell Host Microbe 8:422–432. <http://dx.doi.org/10.1016/j.chom.2010.10.006>.
  20. Heaton NS, Randall G. 2011. Dengue virus and autophagy. Viruses 3:1332–1341. <http://dx.doi.org/10.3390/v3081332>.
  21. Judith D, Mostowy S, Bourai M, Gangneux N, Elek M, Lucas-Hourani M, Cayet N, Jacob Y, Prévost MC, Pierre P, Tangy F, Zimmer C, Vidalain PO, Couderc T, Lecuit M. 2013. Species-specific impact of the autophagy machinery on Chikungunya virus infection. EMBO Rep 14:534–544. <http://dx.doi.org/10.1038/embor.2013.51>.
  22. Zaitseva E, Yang S-T, Melikov K, Pourmal S, Chernomordik LV. 2010. Dengue virus ensures its fusion in late endosomes using compartment-specific lipids. PLoS Pathog 6:e1001131. <http://dx.doi.org/10.1371/journal.ppat.1001131>.
  23. Gay B, Bernard E, Solignat M, Chazal N, Devaux C, Briant L. 2012. pH-dependent entry of chikungunya virus into *Aedes albopictus* cells. Infect Genet Evol 12:1275–1281. <http://dx.doi.org/10.1016/j.meegid.2012.02.003>.
  24. Poh MK, Shui G, Xie X, Shi P-Y, Wenk MR, Gu F. 2012. U18666A, an intra-cellular cholesterol transport inhibitor, inhibits dengue virus entry and replication. Antiviral Res 93:191–198. <http://dx.doi.org/10.1016/j.antiviral.2011.11.014>.
  25. Shi J, Luo H. 2012. Interplay between the cellular autophagy machinery and positive-stranded RNA viruses. Acta Biochim Biophys Sin 44:375–384. <http://dx.doi.org/10.1093/abbs/gms010>.
  26. Marquardt MT, Phalen T, Kielian M. 1993. Cholesterol is required in the exit pathway of Semliki Forest virus. J Cell Biol 123:57–65. <http://dx.doi.org/10.1083/jcb.123.1.57>.
  27. Wu M, Sun LV, Vamathevan J, Riegler M, Deboy R, Brownlie JC, McGraw EA, Martin W, Esser C, Ahmadijnad N, Wiegand C, Madupu R, Beanan MJ, Brinkac LM, Daugherty SC, Durkin AS, Kolonay JF, Nelson WC, Mohamoud Y, Lee P, Berry K, Young MB, Utterback T, Weidman J, Nierman WC, Paulsen IT, Nelson KE, Tettelin H, O'Neill SL, Eisen JA. 2004. Phylogenomics of the reproductive parasite *Wolbachia pipiensis* wMel: a streamlined genome overrun by mobile genetic elements. PLoS Biol 2:E69. <http://dx.doi.org/10.1371/journal.pbio.0020069>.
  28. Hobson RP. 1935. On a fat-soluble growth factor required by blow-fly larvae: identity of the growth factor with cholesterol. Biochem J 29:2023. <http://dx.doi.org/10.1042/bj0292023>.
  29. Caragata EP, Rances E, Hedges LM, Gofton AW, Johnson KN, O'Neill SL, McGraw EA. 2013. Dietary cholesterol modulates pathogen blocking by *Wolbachia*. PLoS Pathog 9:e1003459. <http://dx.doi.org/10.1371/journal.ppat.1003459>.
  30. Voronin D, Cook DA, Steven A, Taylor MJ. 2012. Autophagy regulates *Wolbachia* populations across diverse symbiotic associations. Proc Natl Acad Sci U S A 109:E1638–E1646. <http://dx.doi.org/10.1073/pnas.1203519109>.
  31. Teixeira L, Ferreira A, Ashburner M. 2008. The bacterial symbiont *Wolbachia* induces resistance to RNA viral infections in *Drosophila melanogaster*. PLoS Biol 6:E2. <http://dx.doi.org/10.1371/journal.pbio.1000002>.
  32. Kudchodkar SB, Levine B. 2009. Viruses and autophagy. Rev Med Virol 19:359–378. <http://dx.doi.org/10.1002/rmv.630>.
  33. Scheitz CJ, Guo Y, Early AM, Harshman LG, Clark AG. 2013. Heritability and inter-population differences in lipid profiles of *Drosophila melanogaster*. PLoS One 8:e72726. <http://dx.doi.org/10.1371/journal.pone.0072726>.
  34. Bonizzoni M, Gasperi G, Chen X, James AA. 2013. The invasive mosquito species *Aedes albopictus*: current knowledge and future perspectives. Trends Parasitol 29:460–468. <http://dx.doi.org/10.1016/j.pt.2013.07.003>.
  35. Bhatt S, Gething PW, Brady OJ, Messina JP, Farlow AW, Moyes CL, Drake JM, Brownstein JS, Hoen AG, Sankoh O, Myers MF, George DB, Jaenisch T, Wint GR, Simmons CP, Scott TW, Farrar JJ, Hay SI. 2013. The global distribution and burden of dengue. Nature 496:504–507. <http://dx.doi.org/10.1038/nature12060>.
  36. Burt FJ, Rolph MS, Rulli NE, Mahalingam S, Heise MT. 2012. Chikungunya: a re-emerging virus. Lancet 379:662–671. [http://dx.doi.org/10.1016/S0140-6736\(11\)60281-X](http://dx.doi.org/10.1016/S0140-6736(11)60281-X).
  37. Sommer U, Herscovitz H, Welty FK, Costello CE. 2006. LC-MS-based method for the qualitative and quantitative analysis of complex lipid mixtures. J Lipid Res 47:804–814. <http://dx.doi.org/10.1194/jlr.M500506-JLR200>.
  38. Southam AD, Payne TG, Cooper HJ, Arvanitis TN, Viant MR. 2007. Dynamic range and mass accuracy of wide-scan direct infusion nano-electrospray Fourier transform ion cyclotron resonance mass spectrometry-based metabolomics increased by the spectral stitching method. Anal Chem 79:4595–4602. <http://dx.doi.org/10.1021/ac062446p>.
  39. Viant MR, Sommer U. 2013. Mass spectrometry based environmental metabolomics: a primer and review. Metabolomics 9:S144–S158.
  40. O'Neill SL, Pettigrew M, Sinkins SP, Braig HR, Andreadis TG, Tesh RB. 1997. *In vitro* cultivation of *Wolbachia pipiensis* in an *Aedes albopictus* cell line. Insect Mol Biol 6:33–39. <http://dx.doi.org/10.1046/j.1365-2583.1997.00157.x>.
  41. Molloy JC, Sinkins SP. 2015. *Wolbachia* do not induce reactive oxygen species-dependent immune pathway activation in *Aedes albopictus*. Viruses 7:4624–4639. <http://dx.doi.org/10.3390/v7082836>.
  42. Gluzov EA, Pheasant M, McGraw EA, Bejerano G, Mattick JS. 2005. Ultraconserved elements in insect genomes: a highly conserved intronic sequence implicated in the control of homothorax mRNA splicing. Genome Res 15:800–808. <http://dx.doi.org/10.1101/gr.3545105>.
  43. Weber RJ, Southam AD, Sommer U, Viant MR. 2011. Characterization of isotopic abundance measurements in high resolution FT-ICR and Orbitrap mass spectra for improved confidence of metabolite identification. Anal Chem 83:3737–3743. <http://dx.doi.org/10.1021/ac2001803>.
  44. Kirwan JA, Weber RJM, Broadhurst DI, Viant MR. 2014. Direct infusion mass spectrometry metabolomics dataset: a benchmark for data processing and quality control. Sci Data 1:140012. <http://dx.doi.org/10.1038/sdata.2014.12>.
  45. Tautenhahn R, Boettcher C, Neumann S. 2008. Highly sensitive feature detection for high resolution LC/MS. BMC Bioinformatics 9:504. <http://dx.doi.org/10.1186/1471-2105-9-504>.
  46. Dunn WB, Broadhurst D, Brown M, Baker PN, Redman CW, Kenny LC, Kell DB. 2008. Metabolic profiling of serum using ultra performance liquid chromatography and the LTQ-Orbitrap mass spectrometry system. J Chromatogr B 871:288–298. <http://dx.doi.org/10.1016/j.jchromb.2008.03.021>.
  47. Benjamini Y, Hochberg Y. 1995. Controlling the false discovery rate—a practical and powerful approach to multiple testing. J R Stat Soc Series B Stat Methodol 57:289–300.
  48. Weber RJ, Viant MR. 2010. MI-Pack: increased confidence of metabolite identification in mass spectra by integrating accurate masses and metabolic pathways. Chem Intel Lab Syst 104:75–82. <http://dx.doi.org/10.1016/j.chemolab.2010.04.010>.
  49. Kanehisa M, Goto S, Sato Y, Kawashima M, Furumichi M, Tanabe M. 2014. Data, information, knowledge and principle: back to metabolism in KEGG. Nucleic Acids Res 42:D199–D205. <http://dx.doi.org/10.1093/nar/gkt1076>.
  50. Fahy E, Sud M, Cotter D, Subramaniam S. 2007. LIPID MAPS online tools for lipid research. Nucleic Acids Res 35:W606–W612. <http://dx.doi.org/10.1093/nar/gkm324>.
  51. Fahy E, Subramaniam S, Murphy RC, Nishijima M, Raetz CR, Shimizu T, Spener F, van Meer G, Wakelam MJ, Dennis EA. 2009. Update of the LIPID MAPS comprehensive classification system for lipids. J Lipid Res 50:S9–S14. <http://dx.doi.org/10.1194/jlr.R800095-JLR200>.
  52. Khoo C, Venard C, Fu Y, Mercer D, Dobson S. 2013. Infection, growth and maintenance of *Wolbachia pipiensis* in clonal and non-clonal *Aedes*

- albopictus* cell cultures. Bull Entomol Res 103:251–260. <http://dx.doi.org/10.1017/S0007485312000648>.
53. Lu P, Bian G, Pan X, Xi Z. 2012. Wolbachia induces density-dependent inhibition to dengue virus in mosquito cells. PLoS Negl Trop Dis 6:e1754. <http://dx.doi.org/10.1371/journal.pntd.0001754>.
  54. Hsu F-F, Turk J. 2002. Characterization of ceramides by low energy collisional-activated dissociation tandem mass spectrometry with negative-ion electrospray ionization. J Am Soc Mass Spectrom 13:558–570. [http://dx.doi.org/10.1016/S1044-0305\(02\)00358-6](http://dx.doi.org/10.1016/S1044-0305(02)00358-6).
  55. Rietveld A, Neutz S, Simons K, Eaton S. 1999. Association of sterol- and glycosylphosphatidylinositol-linked proteins with *Drosophila* raft lipid microdomains. J Biol Chem 274:12049–12054. <http://dx.doi.org/10.1074/jbc.274.17.12049>.
  56. Zheng W, Kollmeyer J, Symolon H, Momin A, Munter E, Wang E, Kelly S, Allegood JC, Liu Y, Peng Q, Ramaraju H, Sullards MC, Cabot M, Merrill AH. 2006. Ceramides and other bioactive sphingolipid backbones in health and disease: lipidomic analysis, metabolism and roles in membrane structure, dynamics, signaling and autophagy. BBA Biomembranes 1758:864–1884.
  57. van Meer G, Voelker DR, Feigenson GW. 2008. Membrane lipids: where they are and how they behave. Nat Rev Mol Cell Biol 9:112–124. <http://dx.doi.org/10.1038/nrm2330>.
  58. Carvalho M, Schwudke D, Sampaio JL, Palm W, Riezman I, Dey G, Gupta GD, Mayor S, Riezman H, Shevchenko A, Kurzchalia TV, Eaton S. 2010. Survival strategies of a sterol auxotroph. Development 137:3675–3685. <http://dx.doi.org/10.1242/dev.044560>.
  59. Hannich JT, Umebayashi K, Riezman H. 2011. Distribution and functions of sterols and sphingolipids. Cold Spring Harb Perspect Biol 3:a004762. <http://dx.doi.org/10.1101/cshperspect.a004762>.
  60. Cho K-O, Kim G-W, Lee O-K. 2011. Wolbachia bacteria reside in host Golgi-related vesicles whose position is regulated by polarity proteins. PLoS One 6:e22703. <http://dx.doi.org/10.1371/journal.pone.0022703>.
  61. Lafont F, Van Der Goot FG. 2005. Bacterial invasion via lipid rafts. Cell Microbiol 7:613–620. <http://dx.doi.org/10.1111/j.1462-5822.2005.00515.x>.
  62. Jiang W, Ogretmen B. 2014. Autophagy paradox and ceramide. Biochim Biophys Acta 1841:783–792. <http://dx.doi.org/10.1016/j.bbali.2013.09.005>.
  63. Sentelle RD, Senkal CE, Jiang W, Ponnusamy S, Gencer S, Selvam SP, Ramshesh VK, Peterson YK, Lemasters JJ, Szulc ZM, Bielawski J, Ogretmen B. 2012. Ceramide targets autophagosomes to mitochondria and induces lethal mitophagy. Nat Chem Biol 8:831–838. <http://dx.doi.org/10.1038/nchembio.1059>.
  64. Di Paolo G, De Camilli P. 2006. Phosphoinositides in cell regulation and membrane dynamics. Nature 443:651–657. <http://dx.doi.org/10.1038/nature05185>.
  65. Hilbi H. 2006. Modulation of phosphoinositide metabolism by pathogenic bacteria. Cell Microbiol 8:1697–1706. <http://dx.doi.org/10.1111/j.1462-5822.2006.00793.x>.
  66. Weber SS, Ragaz C, Hilbi H. 2009. Pathogen trafficking pathways and host phosphoinositide metabolism. Mol Microbiol 71:1341–1352. <http://dx.doi.org/10.1111/j.1365-2958.2009.06608.x>.
  67. Pendaries C, Tronchere H, Arbibe L, Mounier J, Gozani O, Cantley L, Fry MJ, Gaits-Iacovoni F, Sansonetti PJ, Payrastre B. 2006. PtdIns(5)P activates the host cell PI3-kinase/Akt pathway during *Shigella flexneri* infection. EMBO J 25:1024–1034. <http://dx.doi.org/10.1038/sj.emboj.7601001>.
  68. Geiger O, Lopez-Lara IM, Sohlenkamp C. 2013. Phosphatidylcholine biosynthesis and function in bacteria. Biochim Biophys Acta 1831:503–513. <http://dx.doi.org/10.1016/j.bbali.2012.08.009>.
  69. Heung LJ, Luberto C, Del Poeta M. 2006. Role of sphingolipids in microbial pathogenesis. Infect Immun 74:28–39. <http://dx.doi.org/10.1128/IAI.74.1.28-39.2006>.
  70. Heaton NS, Randall G. 2011. Multifaceted roles for lipids in viral infection. Trends Microbiol 19:368–375. <http://dx.doi.org/10.1016/j.tim.2011.03.007>.